Upright emplacement of the Gibraltar slab and the origin of rifting in adjacent foreland and Backarc Basins

Check for updates

Pengfei Ma [1] ✉, Shaofeng Liu [2] ✉, Guillermo Booth-Rea[3], Huiping Zhang [4] & Ting Yang [5]

Back-arc basins in subduction systems usually form following discrete subduction-related extension stages. However, in the westernmost Mediterranean, the initiation of Cenozoic extension associated with the Valencia Trough and Algerian Sea Basin introduced two extension centers nearly simultaneously in the Gibraltar subduction system, and this presents a challenge to understanding their underlying dynamics. We built three-dimensional time-dependent geodynamic models constrained by tectonic reconstructions to determine the role that the Gibraltar subduction played in shaping unconventional extensional basins. Our results suggest that the Algerian Sea Basin is a typical back-arc basin, whereas the Valencia Trough opened on the subducting plate during the rotational rollback of the Gibraltar slab. Moreover, the Valencia Trough extension likely delayed slab tearing and guided slab sinking before its final detachment, facilitating its ultimate upright positioning. We show how plates and the mantle interact dynamically in a subduction system where the slab asymmetrically rolls back.

Subduction is a primary driver of plate tectonics[1,2], as it substantially influences the way the lithosphere deforms near plate boundaries[3–6]. Despite subduction occurring within overall convergent settings, localized extensional deformation frequently occurs in these systems under slab-pull forces or due to lateral crustal density heterogeneity within the subducting plate[7–9]. The link between extension and subduction is often unstable, and is potentially marked by the formation of a group of back-arc basins after the spreading center jumps[10] due to mechanisms, such as slab tear propagation[11], mantle plume activity[12], or interactions between the descending slab and the 660 km discontinuity[13]. Spatially, these shifts in extension usually move sequentially toward trenches (e.g., the subbasins in the Philippine Sea plate[14] and the Liguro-Provencal and Tyrrhenian Basins in the central Mediterranean region[10,15]). Occasionally, they may migrate toward the overriding plates (e.g., the Norfolk and Lau Basins[12]). Regardless of the direction in which these shifts migrate, extension pulses, which create rift basins, are typically successive and do not overlap temporally.

However, this sequential pattern of extensional shifting is not evident in the rift basins of the westernmost Mediterranean region[16,17]. Traditionally, the neighboring Valencia Trough and the Algerian Sea Basin, have been considered back-arc basins associated with Gibraltar or Tell subduction[18–21]

(Fig. 1, Supplementary Note 1). Geological evidence indicates that the peak Cenozoic extensional phase of the Valencia Trough commenced in the late Oligocene and ceased due to a thrusting event in the early Miocene[22–24]. Further extension followed in the Balearic promontory thickened crust in the middle Miocene[25] (Fig. 1). In contrast, rather than following the typical sequential and temporally distinct extensional migrating basin formation described above, the extension of the Algerian Sea Basin, which has been traced to the initial extension of the Alboran Domain further west (Fig. 1), is suggested to have persisted from the early Oligocene until the late Miocene[26–29]. Thus, the coeval extension of the Valencia Trough and the Algerian Sea Basin within one subduction system challenges our current understanding of back-arc basins. Additionally, clarifying how Gibraltar or Tellian slab subduction could result in two simultaneous extensional centers, i.e., basins, presents a challenge. Therefore, it is necessary to understand the early history of the Westernmost Mediterranean and especially, the Gibraltar subduction zone.

Nevertheless, seismic tomographic models reveal the noncylindrical shape of the present Gibraltar slab, whose detached part interestingly appears to show an upright orientation rather than lying flat above the 660 km discontinuity beneath the Betics[30,31] (Fig. 1), hindering the slab

[1]College of Geosciences and Survey Engineering, Taiyuan University of Technology, Taiyuan, China. [2]State Key Laboratory of Geological Processes and Mineral Resources, Frontiers Science Center for Deep-time Digital Earth, and School of Earth Sciences and Resources, China University of Geosciences (Beijing), Beijing, China. [3]Department of Geodynamics, University of Granada-Instituto Andaluz de Ciencias de la Tierra (CSIC), Granada, Spain. [4]State Key Laboratory of Earthquake Dynamics, Institute of Geology, China Earthquake Administration, Beijing, China. [5]Department of Earth and Space Sciences, Southern University of Science and Technology, Shenzhen, China. ✉e-mail: mapengfei@tyut.edu.cn; shaofeng@cugb.edu.cn
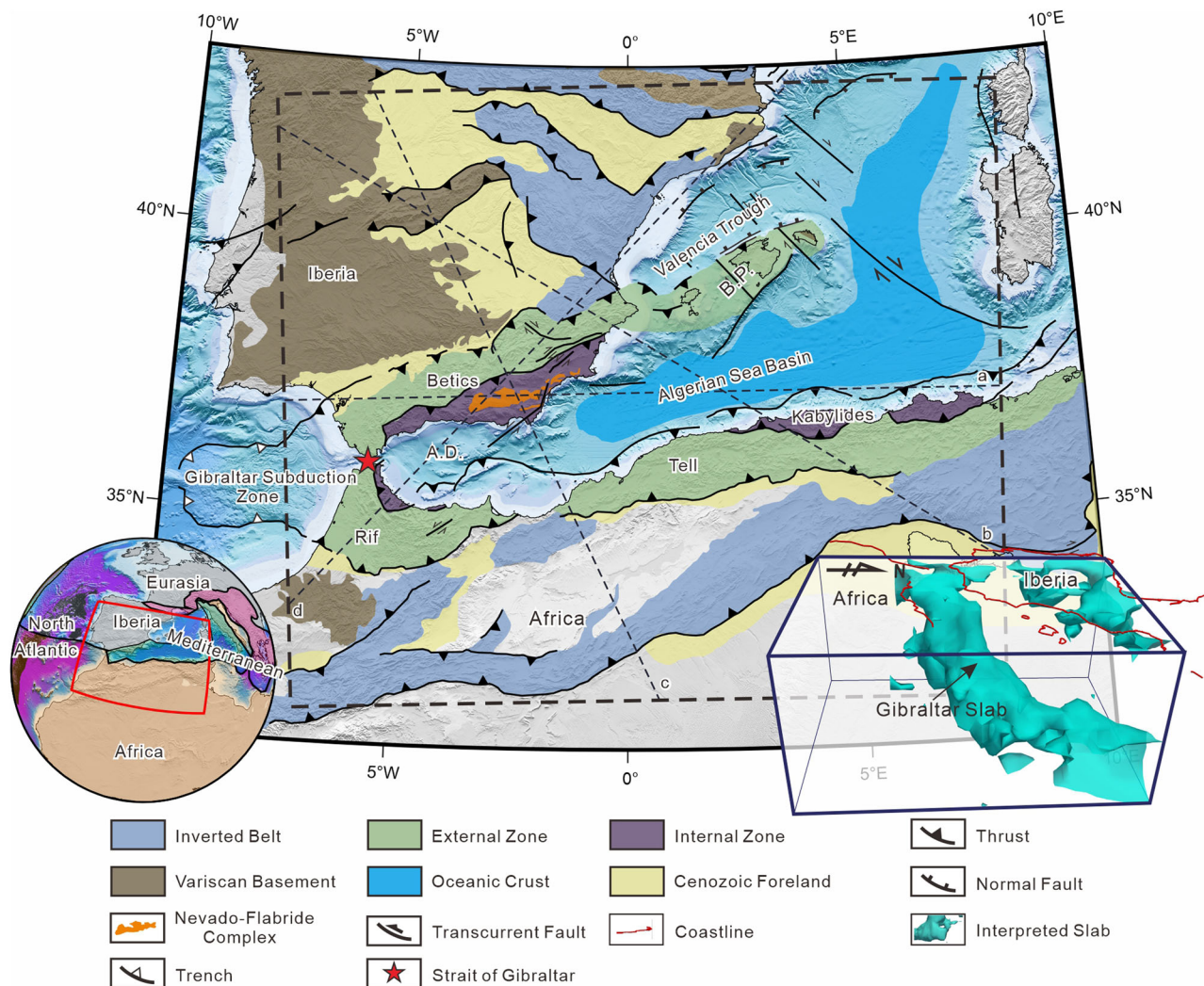
Fig. 1 | Tectonic map of the western Mediterranean region (based on ref. 25). The inset map in the bottom left corner shows the current tectonic settings, with plate tectonic data sourced from the updates of ref.[61] and bathymetric data obtained from the ETOPO1 model[65]. The lower right corner shows the three-dimensional 'standing' Gibraltar slab from the global seismic tomography model UU-P07[31], represented by the cyan surface that outlines the +0.3% contour of the velocity anomaly field. The thick dashed black box on the large map shows the extent of the geodynamic models, whereas the thin dashed black lines represent the locations of the profiles shown in Fig. 3 and Supplementary Fig. 1. The red star denotes the Strait of Gibraltar. Abbreviations: A.D. = Alboran Domain; B.P. = Balearic Promontory.

emplacement reconstruction[21]. Previous researchers have proposed different tectonic reconstruction models[20,32,33] (Supplementary Note 2), but identifying the most plausible model remains challenging[17].

Three-dimensional forward geodynamic models have proven to be powerful tools for studying subduction zone evolution. This approach has been adopted by several researchers to study the evolution of the Gibraltar subduction zone. Chertova et al.[34] reconstructed the evolution of the Gibraltar subduction with forward geodynamic models. In their preferred model, the Gibraltar subduction zone initially subducted northwestward beneath the Baleares and the slab underwent 180° clockwise rotation during the subsequent rollback. Peral et al.[35] built 3D numerical models to explore the possibility of another scenario with two independent opposing subduction systems (the Gibraltar slab and the Liguro-Tethys slab). Recently, Duarte et al.[36] built a series of new numerical models. Their models are supported by a wealth of observations, such as seismic tomography, SKS splitting and emplacement of the Beni Boussera and Ronda subcontinental peridotite bodies. They even made predictions about the future evolutionary trends of the Gibraltar subduction zone, which provides more details on the development of subduction invasion[36].

Although considerable research has focused on the evolution of the Gibraltar subduction zone, its connection to the development of the two neighboring rift basins has not been well addressed. Furthermore, the vertical emplacement of the detached Gibraltar slab itself has not received enough attention. Whether this intriguing phenomenon is related to the regional crustal deformation pattern also needs to be addressed.

To determine the role of the Gibraltar subduction in shaping unconventional extensional basins and reconstruct the evolution of the vertical Gibraltar slab, we attempted to reconstruct a feasible history within a unified plate–mantle system by formulating a series of time-dependent 3D geodynamic models based on tectonic reconstructions. The model predictions highlight the comprehensive interplay between the extension of the Algerian Sea Basin and the Valencia Trough and the asymmetrical rollback of the Gibraltar slab.

Results and discussion

We collected four representative reconstruction models from published studies, namely, V14[20], V12[21], R22[17], and S04[33] (Methods; Fig. 2). Additionally, we created a new model based on the S04 model to consider the influence of a preexisting weak zone near the Iberian continental margin at the present location of the Valencia Trough on the evolution of the Gibraltar subduction zone, which may have further affected the crustal deformation pattern. We refer to the new model as M23 (Methods; Fig. 2a). A set of 3D
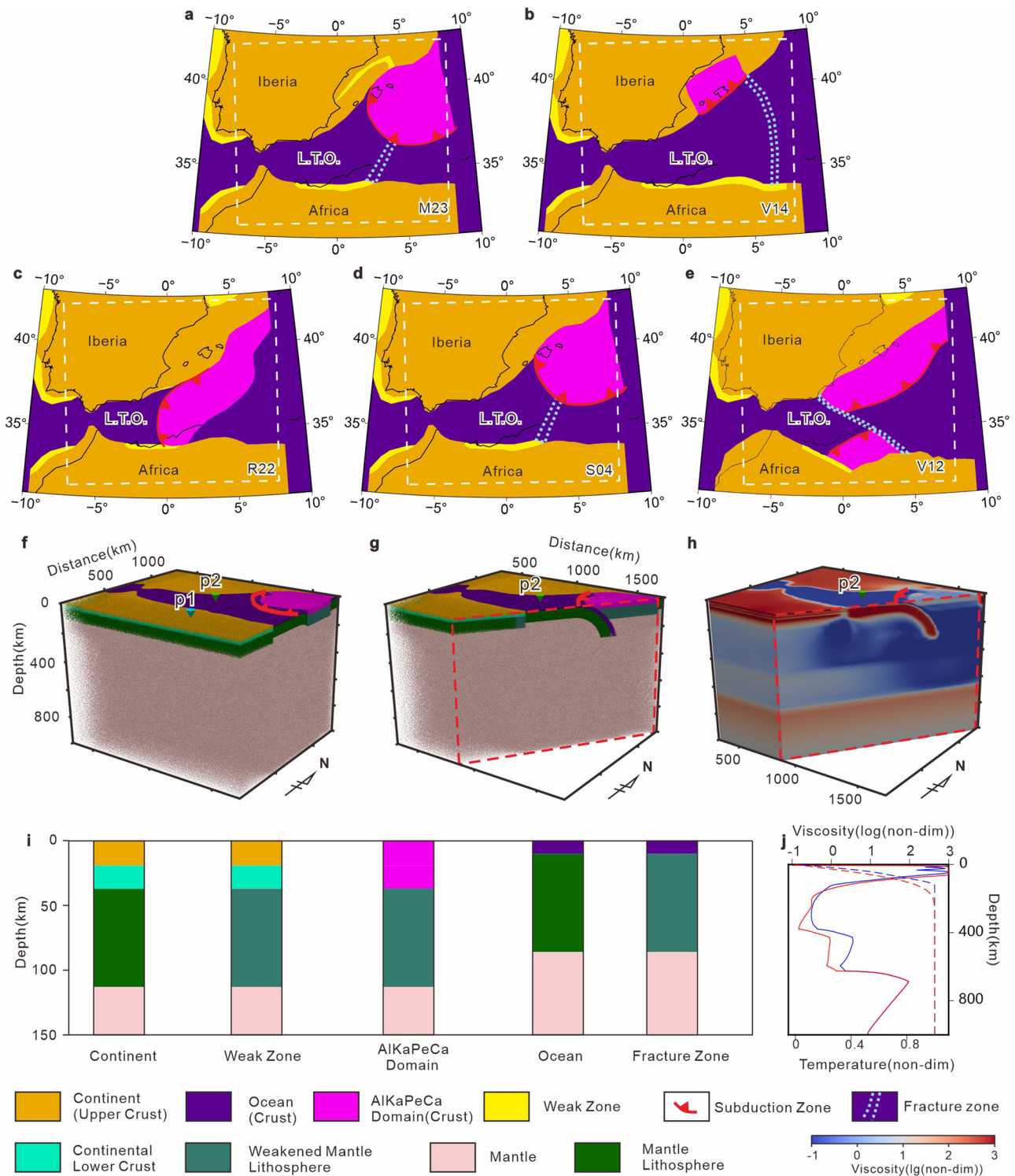
Fig. 2 | Initial settings for the three-dimensional geodynamic model cases constrained by tectonic reconstructions. a–e Digitalized plate reconstructions. The white dashed boxes show the extents of the geodynamic models. The thin black lines represent present-day coastlines. Abbreviations for the reconstructions were assigned on the basis of the first letter of the first author's name and the year of paper publication, as follows: V14 is van Hinsbergen et al. [20]; V12 is Vergés and Fernàndez[21]; R22 is Romagny et al.[17]; S04 is Spakman and Wortel[33]; and M23 is this study. Note that the main difference between M23 and S04 is in the weak zone, as indicated by the yellow area, which is behind the eastern Iberian margin. **f–j** Initial material, viscosity and temperature fields of the geodynamic model illustrated by Case 1-1, which is constrained by M23. **f** Initial material field and two sampling points, p1 and p2, which correspond to the positions of continental and oceanic lithospheres, respectively. These sampling points are indicated by the blue and red lines in (**j**). **g, h** Initial material field and viscosity field, respectively, represented by an arbitrary profile perpendicular to the trench. **i** Typical compositional columns for different tectonic units above a depth of 150 km. The AlKaPeCa Domain, a conceptual geological entity on the overriding plate that was later dismembered by subduction[20], has the same composition as the normal continental crust; however, its crust is highlighted in magenta for better visual identification. **j** Initial viscosity and temperature curves sampled vertically across the model from p1 and p2 in Case 1-1. The dashed lines represent temperature fields, whereas the solid lines represent viscosity fields. The blue lines correspond to p1, and the red lines correspond to p2. Abbreviations: L.T.O. = Liguro-Tethys Ocean.

Fig. 3 | Three-dimensional views of the predicted Gibraltar slab structure for Case Series 1-1, 2-1, 3-1, 4-1, and 5-1, which were guided by different tectonic reconstructions but shared the same set of physical parameters. The subducted slabs and the bottom of the continental lithosphere are illustrated as dark blue surfaces, represented by the envelope of lithospheric material particles. The red lines on the top surface represent the coastlines. The black arrows indicate the true north. Annotations include the name of the case (in black) and the corresponding model runtime from the initial to the final state (in red). The transparent light green horizontal planes indicate the 660 km depth. Panels (**a, b**) show the views for Case 1-1 at 22.0 Myr; (**c, d**) for Case 2-1 at 25.0 Myr; (**e, f**) for Case 3-1 at 21.1 Myr; (**g, h**) for Case 4-1 at 20.9 Myr; and (**i, j**) for Case 5-1 at 17.3 Myr.
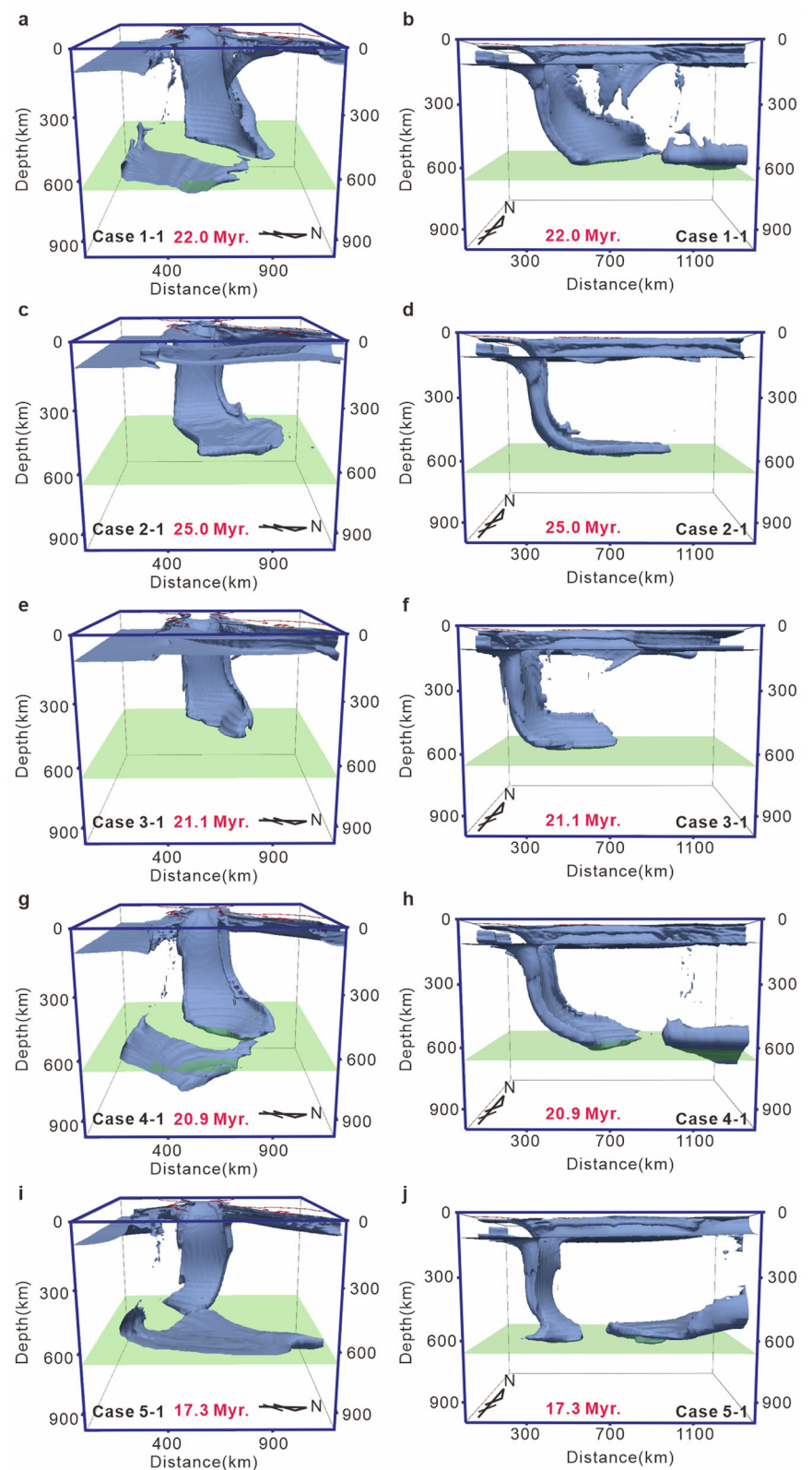

geodynamic model cases (Cases 1-1, 2-1, 3-1, 4-1 and 5-1) were subsequently built on the basis of these reconstruction models (Methods; Fig. 2 and Supplementary Tables 1 and 2). This set of model cases were designed to test the feasibility of each of the reconstruction models and reconstruct a plausible history of the Gibraltar subduction zone. Additionally,

the influence of lower mantle viscosity (Cases 1-1, 1-2, and 1-3), activation volume (Cases 1-4, 1-5, 1-6, 1-7, 2-2 and 2-3) and crust yield coefficient (Cases 1-1, 1-8, and 1-9) on slab behavior, which are guided by reconstruction models M23 and V14 (Supplementary Table 2), were explored.

Fig. 4 | Correspondence between the predicted slab structure of Case 1-1 and seismic tomography model UU-P07 along four profiles. The slab morphology is depicted by dark green curves and are defined by temperature contours 15% lower than the ambient mantle temperature. The slab contours are superimposed over the tomographic slices. The quantified comparison results in each profile (R1 and R2 scores) are annotated in the lower right corner of each subfigure. The small white circles indicate National Earthquake Information Center (NEIC) seismicity from 30 October 1999 to 21 October 2022 within a 30 km range on each side of the profile. The top profile with blue polygons in each subfigure shows the topography and bathymetry information, and the location of corresponding key tectonic features are denoted. Panel **a** shows the predicted slab structure and tomography slice for profile a; **b** for profile b; **c** for profile c; and **d** for profile d. The profile locations are shown in Fig. 1.
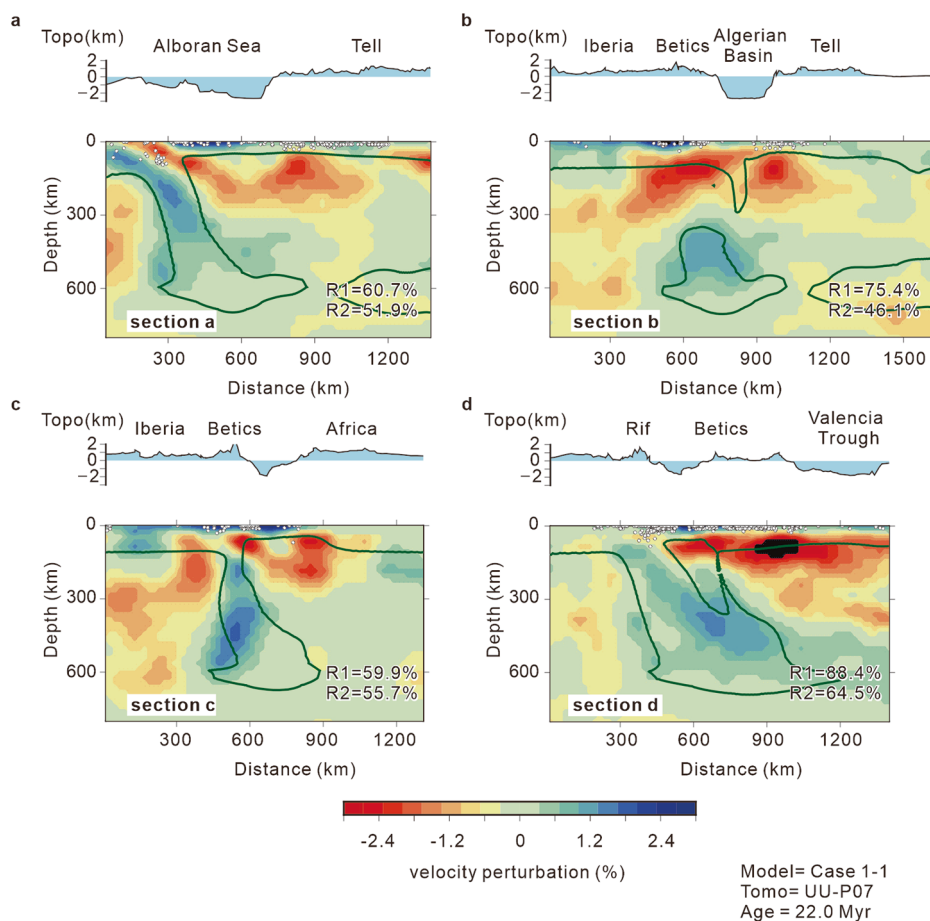
Evaluation of predictions from different model cases

We evaluated various numerical model cases by comparing their predictions with available observations. These observations comprised the slab architecture interpreted from seismic tomography models UU-P07[31] and IBEM-P18[37], the present-day tectonic map (Fig. 1), and the implied history of surficial deformation derived from recorded tectonic events (Supplementary Table 3). Along with qualitative comparisons, we conducted quantitative analyses to assess the degree of overlap between the predicted present slab and high-velocity anomalies in seismic tomography model UU-P07, using the R1/R2 score in the profiles (see the "*Quantitative validation of model predictions*" section in the Methods).

These geodynamic model cases achieve different degrees of correspondence with the observations. For example, Case 3-1, constrained by R20[17], successfully reproduces the position, orientation, and morphology of the slab (Fig. 3e, f, Supplementary Figs. 1 and 2), and achieves higher scores (average of 85.4% for the R_1 score and 49.8% for the R_2 score across all four profiles) against the UU-P07 model in quantitative assessments (Methods; Supplementary Fig. 3 and Supplementary Table 4). However, this model fails to capture the Balearic Promontory and the Valencia Trough in its predicted surface structures and tectonic events (Supplementary Figs. 4a, d and 5).

Conversely, some of the model cases constrained by M23 (Cases 1-2 and 1-3) yielded surficial deformation patterns that were consistent with geological records (Supplementary Figs. 6, 7b and c and Supplementary Table 3). However, these cases predicted a Gibraltar slab lying flat above the 660 km discontinuity (Supplementary Figs. 8c–f, 9) rather than a vertical slab from tomographic models. This mismatch results in a low R_2 score as low as 35% for profiles b and d (Supplementary Fig. 3 and Supplementary Table 4).

Model cases (Cases 2-1 and 2-2) constrained by the V14 model, which was preferred by previous researchers, predicted a massive steeply ENE dipping Gibraltar slab (Supplementary Figs. 10 and 11) and a large back-arc basin above the slab (Supplementary Fig 11 and 12), which is obviously inconsistent with the regional tectonics (Fig. 1).

Some model cases (Cases 1-6, 1-7, 2-3, 4-1 and 5-1) failed both to replicate the observed surface tectonic features and events (Supplementary Figs. 4, 7 and 13) and to predict the noncylindrical Gibraltar slab (Fig. 3g–j and Supplementary Figs 10e, f and 14g–j). Models with high activation volumes (larger than $6.0 \times 10^{-6} m^3/mol$) typically predict slower subduction processes and trench retreat rates, such that after 30 Myr of model running, the Gibraltar trench has not yet reached its current position (Supplementary Fig. 14g–j).

Most model cases constrained by tectonic reconstruction model M23, especially Case 1-1, exhibited predictions that were more consistent with the present surface tectonics (Fig. 1 and Supplementary Fig. 7) and past tectonic events (Supplementary Figs. 15 and 16, Supplementary Note 1), such as the NW-SE extension of the Valencia Trough (Supplementary Fig. 15b, c), the shortening (Supplementary Fig. 15d) and subsequent extension (Supplementary Fig. 15f) in the Betics, and the two phases of extension and intervening shortening of the Balearic Promontory (Supplementary Fig. 15b-e). Cases 1-4 and 1-5 predict deformation histories similar to those of Case 1-1 (Supplementary Fig. 17, 18), but longer times, up to 30 million years, from the initial to the final state, are needed for these cases. Furthermore, Cases 1-1, 1-4, 1-5, 1-8 and 1-9 predict upright slab conditions that agrees with the tomographic models (Fig. 4 and Supplementary Figs. 3, 14a–f and 17–20), and they generally achieve higher R_2 scores in profiles b to d in the quantitative validation process (Supplementary Fig. 3b–d and Supplementary Table 4) than model cases that predict a flat-lying Gibraltar slab (Cases 1-2 and 1-3, Supplementary Figs. 3 and 9).
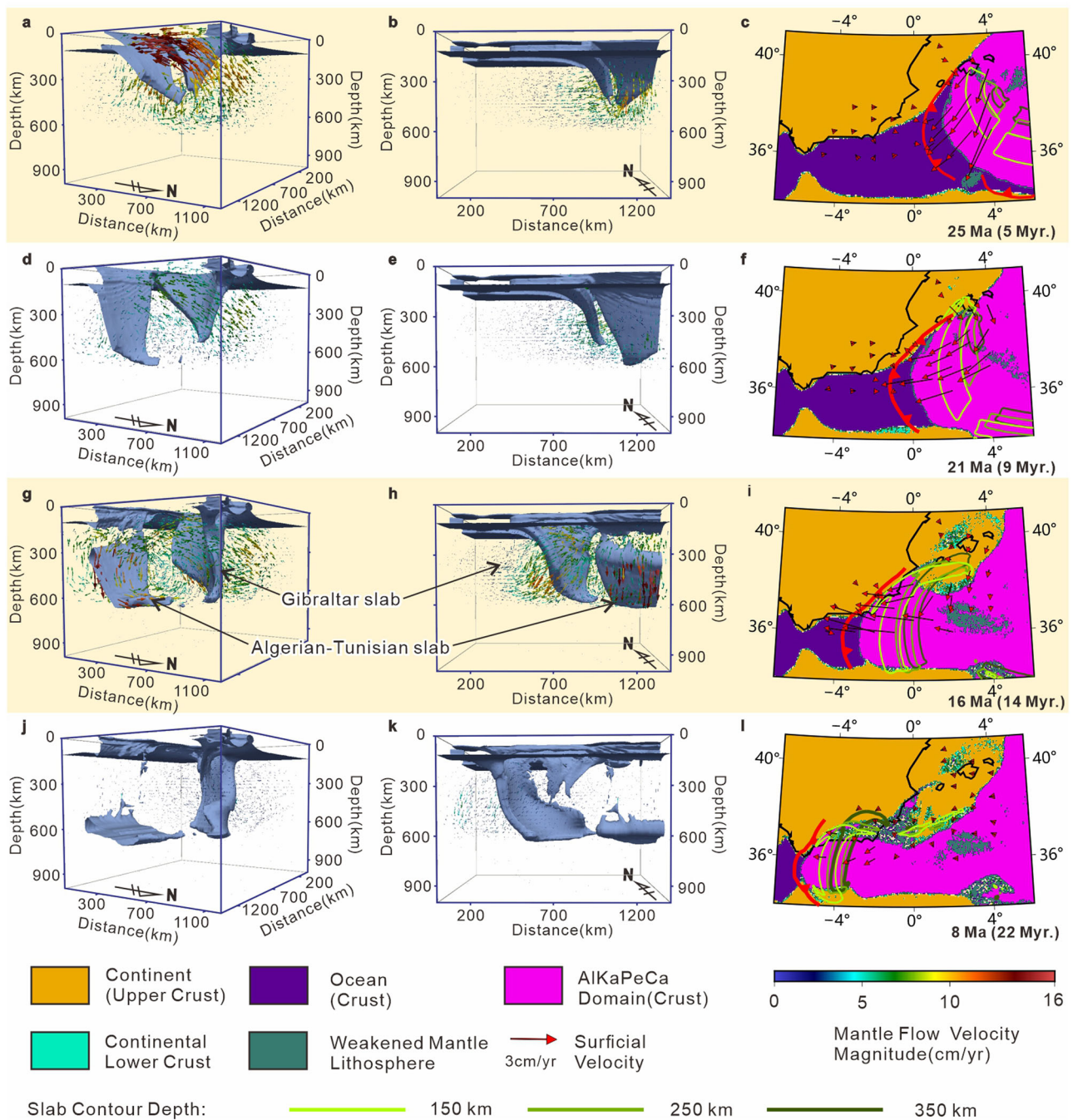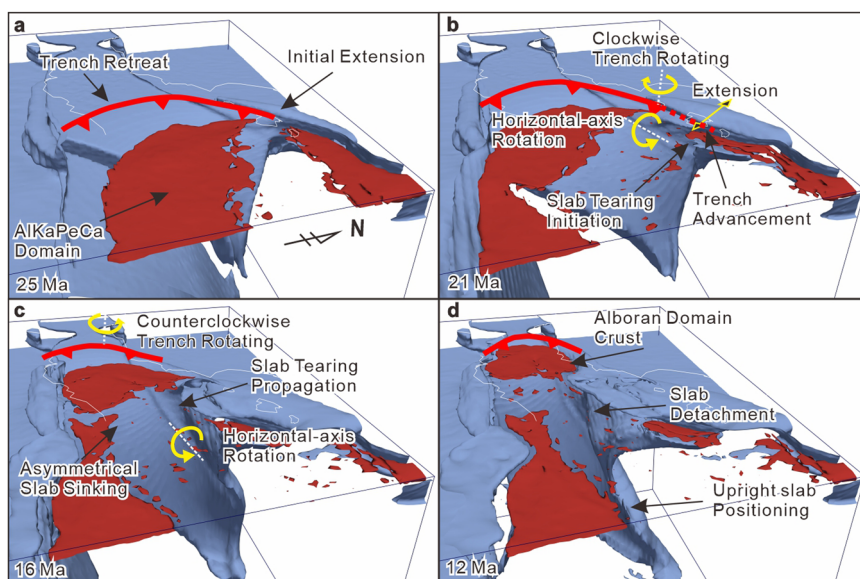
Fig. 5 | The evolution of the plate-mantle system in the westernmost Mediterranean from late Oligocene to late Miocene predicted by Case 1-1. Panels (**a–c**) show the slab architecture and corresponding surface tectonics at 25 Ma; (**d–f**) at 21 Ma; (**g–i**) at 16 Ma; (**j–l**) at 8 Ma. Geological ages and model runtimes (in parentheses) are noted in the lower right corner of each row. Panels (**a, d, g, j**) show the three-dimensional morphology of the Gibraltar slab from a northeast to southwest perspective, while panels (**b, e, h, k**) offer a view from south to north. The slabs and the bottom of the continental lithosphere are represented by dark blue surfaces, defined by the envelope of the lithospheric material. Colored vectors indicate the mantle flow state, with the color bar in the lower right corner showing the velocity magnitude of the mantle flow. The black arrows indicate the true north. Panels (**c, f, i, l**) present map views of the predicted trench and surficial tectonics. Red sawtooth lines represent the trench, with the teeth pointing toward the subduction polarity. Red arrows depict the predicted local surface velocity. Slab morphology is shown by depth contour lines, with colors indicating different depths. Please refer to the color of the lines at the bottom for the slab contour depth. Present-day coastlines are delineated by solid black lines.

Overall, we chose Case 1-1 as the reference model because it demonstrated better agreement between the predictions and observations for both the Gibraltar slab architecture (Fig. 4, Supplementary Figs. 3 and 18) and surface tectonics in the Betic-Balearic region (Supplementary Fig. 4b and 16; Supplementary Note 3). However, it should be noted that the geodynamic models in this study focus solely on the subduction process, which is a simplification of the western Mediterranean Nubia-Eurasia plate convergence setting. In addition, owing to the limited model dimensions and simplified boundary conditions, Case 1-1 achieved only a first-order approximation. Many detailed predictions are inconsistent with observations, such as compression in the Valencia Trough at 9 Ma and detachment of Algerian-Tunisian slab at 16 Ma (Fig. 5g, h).

Fig. 6 | Gibraltar slab rotation and tearing beneath the Iberian margin in a 3D magnified view. The red areas represent the dismembered AlKaPeCa Domain crust, whereas the blue surfaces represent the envelope surface of the lithospheric mantle. The yellow arrows indicate slab rotation and lithospheric extension. The geological age is shown in the lower left corner of each subfigure. All the data are derived from Case 1-1. **a** Initiation of the subduction process occurred as the continental lithosphere of the Baleares margin entered the Gibraltar subduction zone. **b** The extension of the Valencia Trough inhibited immediate slab tear propagation along the Balearic margin. The imbalance of forces facilitated a unique slab rotational rollback. **c** The westward propagation of tearing altered the manner in which the slab underwent rollback. **d** The tear propagated through the central segment of the southern Iberian margin, resulting in the slab standing above the 660 km discontinuity in the upper mantle. The Alboran Domain separated from the other parts of the AlKaPeCa Domain and migrated westward above the retreating Gibraltar slab between the continents.

Two-stage Gibraltar subduction and its surface expression

To fully grasp the dynamics driving the formation of the Valencia Trough and the Algerian Basin, a comprehensive 3D reconstruction of the plate-mantle system is essential. The predictions from the numerical models, especially Case 1-1, provide a valuable opportunity for the spatiotemporal reconstruction of the Gibraltar subduction and the associated lithospheric deformation. According to Case 1-1, the Gibraltar subduction zone originally formed the western segment of the Ligurian-Tethys subduction zone, exhibiting an ENE polarity (Fig. 2a), and underwent a two-stage evolutionary process. For illustrative purposes, we assumed that Case 1-1 commenced at 30 Ma, probably around 20 million years after first subduction signal, with metamorphic rutile growth at 49.8 ± 1.3 Ma in low-grade Tellian metabasites (Supplementary Table 3). Accordingly, we converted the simulation times into geological ages.

In the earliest stage of Gibraltar subduction, the slab rolled back radially as a part of the Liguro-Tethys subduction system. During this time, the southern segment of the curved Gibraltar subduction zone and the Algerian-Tunisian subduction zone underwent oceanic crust subduction, with the trench retreating progressively westward toward the Strait of Gibraltar and southward toward Africa (Fig. 5a–f). In the northeastern segment of the trench, due to the highly oblique angle between the initial convergence direction and trench orientation, crustal shortening was less pronounced. However, the ongoing subduction and the presence of a weak lithosphere behind the Iberian continental margin initiated the initial NW-SE extension of the Valencia Trough and the Balearic Promontory.

In the earliest Miocene, the Gibraltar slab completely decoupled from the Algerian–Tunisian slab to the east. Following this decoupling, the Algerian–Tunisian slab continued to retreat southward. In contrast, the Gibraltar slab experienced a more complex evolution. The southern segment experienced smooth subduction, due to the the relatively weak coupling between the Liguro-Tethys Ocean (Fig. 2) and the African continent[38], along with the subduction of oceanic lithosphere. However, in the northeastern segment, the buoyant Iberian lithosphere's entry into the subduction channel created a bottleneck, hindering the local subduction process (Fig. 5c, f). This interaction of opposing forces along the trench generated torque, leading to the clockwise rotational rollback of the Gibraltar slab (Fig. 6b). During this rotational subduction, internal deformation of the viscous Gibraltar slab was minimized.

The progressive sinking of the Gibraltar slab into the mantle, coupled with the slab's rotation, introduced a horizontal-axis component around the Iberian margin (Fig. 6b). As a result, the dip angle of the slab rapidly decreased in the southern segment, whereas the slab remained vertically suspended in the northeastern segment. Then the slab widened in the northeastern direction along the overall strike of the trench, with its tip stagnating above the mantle transition zone. Moreover, the vertical-axis component of the slab rotation led to local southeastward advancement at the northeast end of the trench (Figs. 5f and 6b), further inducing asymmetric extension within the continental interior of the subducting plate along preexisting weak zones. This extension ultimately resulted in the formation of a V-shaped basin opening toward the northeast, known as the Valencia Trough.

By the end of the first stage, after the trench had finished a clockwise rotation of approximately 20 degrees, the polarity of the Gibraltar subduction zone had transitioned from ENE to southeastward (Fig. 5d–f). This shift brought the subduction direction nearly perpendicular to the trench, resulting in a more pronounced shortening of the Balearic Promontory along the southeastern margin of the Valencia Trough. (Supplementary Fig. 15c).

At approximately 18 Ma, the lithosphere of the Iberian margin in the northeastern segment began to yield (Fig. 6c). A tear in the Gibraltar slab initiated beneath the eastern end of the Balearic Promontory, triggering localized, small-scale convective cells in the mantle. The rupture of the lithosphere along the Iberian margin induced an important shift in the stress field across the entire system, and the evolution of the Gibraltar subduction period entered the second stage. Subsequently, the small-scale mantle convection cells facilitated the rapid westward propagation of the tearing process. Because of this tearing process, the Gibraltar slab decoupled from the Iberian continental lithosphere and retreated westward. The detached section then sank and diachronously approached the 660 km discontinuity. Induced by sustained horizontal-axis rotation in the first stage, the slab finally turned downward along its flank near the 660 km discontinuity, which corresponds to the tear from the Algerian–Tunisian slab along a presumed fracture zone (Figs. 2a and 5g, h); moreover, the slab turned upward along its tear from the Iberian margin (Fig. 6).

After detachment, the tip of the detached slab underwent a gradual clockwise vertical-axis rotation of approximately 20 degrees at the bottom of the upper mantle while the entire slab continued to retreat westward. This rotation led to a reorientation of the slab from northeast (NE) to east–northeast (ENE) and enhanced its ultimate upright positioning, roughly aligning with the Betic-Rif-Baleares belt (Figs. 5i and 6d). Moreover,

the slab sank to depth greater than 300 km and thickened as a whole under the combined influence of gravity and its own viscous resistance force.

Following the tearing of the Gibraltar slab from the Iberian lithosphere, the sudden cessation of the pulling force of the slab may have contributed to an alteration in the direction of the Balearic Promontory extension from the NE–SW to the NW–SE[25] and weakening of the the extension in the Valencia Trough[39].

As the tearing process progressed, the torque exerted on the slab reversed, inducing a counterclockwise rotation in the trench (Fig. 6c). By the end of the Tortonian (8 Ma), the Gibraltar subduction zone had reverted to its eastward polarity (Fig. 5j-l).

During the rotational rollback of the Gibraltar slab, the lithosphere of the AlKaPeCa Domain (Fig. 2) overriding the slab experienced intensive extension due to rollback-induced toroidal mantle flow[40], leading to pronounced thinning of the crustal basement in the Alboran Domain (Fig. 6d). In turn, this thinning resulted in the formation of the proto-Algerian Basin, presently represented by the West Alboran Basin[28,29] (Figs. 5i, l and 6d).

Therefore, the Algerian Sea Basin and its predecessor, the thinned Alboran Domain in the Western Alboran Basin, correspond to the back-arc domain associated with the Gibraltar subduction zone. Its formation resulted from the intense extension of the AlKa Domain above the narrow Gibraltar slab (Fig. 6d).

In contrast to those in the Algerian Sea Basin, the dynamics governing extension and its subsequent cessation in the Valencia Trough are unconventional, because the Valencia Trough is on the subducting plate rather than the overriding plate. Mechanically, for the extension of the Valencia Trough to occur, specific prerequisites are needed. On the one hand, the weak zones in the subducting plate are necessary (Fig. 2a). On the other hand, lateral variations in stress fields along the trench are necessary for the extension of the Valencia Trough, and these lateral variations typically arise from the heterogeneity of the subducting lithosphere[41].

Under rotational subduction conditions, the extension of the rift basin is asymmetric because of the variation in trench migration velocity. This pattern is supported by geophysical observations, which indicate that the extension in the eastern part of the Valencia Trough is larger than that in the west[19,24,42].

To summarize, the Gibraltar subduction zone underwent a two-stage history, demarcated by the initial tearing of the slab along the Iberian margin near the Balearic Promontory. The first stage is characterized by asymmetric rollback of the slab, clockwise rotation of the trench and extension in the Valencia Trough (Fig. 6b), whereas the second stage is characterized by detachment of the slab from the Iberian continent and counterclockwise rotation of the trench (Fig. 6c). The Valencia Trough developed asymmetrically on the subducting plate due to local trench advancement during the clockwise rotation of the rigid Gibraltar slab.

Factors guiding the upright orientation of the Gibraltar slab

Tomographic models show that the Gibraltar slab has a steeply dipping shape, which generally displays an arcuate shape that is concave toward the east or southeast when viewed in horizontal slices[30,31,43]. In profile, a traverses the Betics belt following an east-west trend, the top of the high-velocity anomaly ascends from a depth of 300 km to near the surface in a westward direction, whereas its bottom reaches the 660 km discontinuity across the profile (Fig. 4a). This 'thick' slab interpreted in a vertical profile implies that the slab is in an upright orientation rather than 'lying' flat above the 660-km discontinuity beneath the Betics orogenic belt (Fig. 1). Seismic tomographic models[31,44,45] suggest that most slabs that stagnate in the upper mantle deflect horizontally at the 660-km discontinuity[46] and that slabs posited upright, like the Gibraltar slab, are extremely rare; thus, it is necessary to explore the key factors that guide this distinctive slab behavior. Therefore, we analyzed the predictions from a set of comparative experimental cases.

Consistent predictions were obtained for Cases 1-1, 1-8, and 1-9 (Supplementary Fig. 20), indicating that the choice of yield coefficient does not markedly impact the slab orientation. The different run times suggest

that an increase in the friction coefficient μ_0 from 0.3 to 0.4 could delay the progress of slab tearing by 1 to 2 million years.

In contrast, the predictions of Cases 1-1, 1-2, and 1-3 reveal obvious differences in terms of the slab orientation (Supplementary Fig. 8). In the Case 1-1 prediction, there is an upright Gibraltar slab, whereas in Cases 1-2 and 1-3, which have a viscosity prefactor smaller than 50 for the lower mantle, a flat-lying Gibraltar slab is predicted. In Cases 1-4, 1-5, 1-6 and 1-7, where the activation volume of the mantle is explored, the viscosities of the lower mantle are always larger than $1 \times 10^{23} \, Pa \cdot s$. The high viscosity of the lower mantle helps maintain the upright position of the Gibraltar slab in Cases 1-4 and 1-5 (Supplementary Figs. 17 and 18). In Cases 1-6 and 1-7, with an activation volume larger than $6 \times 10^{-6} \mathrm{m}^3/\mathrm{mol}$, the subduction process considerably slows (Supplementary Fig. 14). The Gibraltar trench has not reached its final position even by 30 million years, which is inconsistent with the observations (Supplementary Fig. 14g–j). Therefore, a high viscosity lower mantle is necessary to provide sufficient viscous resistance to prevent the slab from slipping during its rotational rollback, allowing it to be securely oriented upright above the 660 km discontinuity.

The most revealing insight into the development of the slab orientation is obtained on the basis of a comparison between Cases 1-1 and 4-1 in which the primary difference in the input parameters lies in whether a weak zone exists at the location of the present-day Valencia Trough. In Case 1-1, an upright slab was predicted (Figs. 3a, b and 6). In contrast, in Case 4-1, a flat-lying Gibraltar slab was predicted (Fig. 3g, h and Supplementary Fig. 21d).

The contrasting predictions of these two cases indicate that the rifting in the Valencia Trough played a crucial role in shaping the current upright configuration of the slab beneath the Betics. The simultaneous extension of the Valencia Trough helped accommodate the pulling force exerted by the Gibraltar slab, preventing immediate detachment from the Balearic Promontory when the Iberian lithosphere entered the subduction channel. After running for 9 Myr, tearing of the Gibraltar slab is clearly visible in Case 4-1 (Supplementary Figs. 21b, 22c). In contrast, in Case 1-1 (where 9 Myr corresponds to 21 Ma), the tearing has just begun (Fig. 6b and Supplementary Fig. 23).

This delay in slab detachment beneath the Balearic Promontory promoted continued coupling between the Liguro-Tethys Ocean and the Iberian continent and facilitated the horizontal rotation of the Gibraltar slab around the Iberian margin (Fig. 6b and c). As a result, the detached slab portion first approached the 660 km discontinuity along its tear with the Algerian–Tunisian slab after a horizontal-axis rotation of approximately 90 degrees and subsequently maintained an upright position above this flank within the upper mantle during rotational rollback. Essentially, the Valencia Trough worked as a "switch" governing early trench rotation and lithosphere tearing, which determined the final behavior of the Gibraltar slab, whether it lied flat or posited upright. This finding suggests a reciprocal influence, where lithospheric deformation responds to subduction processes and affects the behavior of subducting slabs. Thus, the integrated Gibraltar subduction system reveals intricate interactions and mutual influences between the mantle and lithospheric plates.

One exception is Case 3-1, which predicted the slab morphology (Fig. 3e, f and Supplementary Figs. 1 and 2); however, this case failed to precisely predict deformation in the Balearic Promontory and Valencia Trough (Supplementary Fig. 5). This partial success originates from the initial placement of the Gibraltar slab in Case 3-1, which directly considers the appropriate strike and polarity in the second stage without accounting for the early interactions between slab tearing and trench rotation in the first stage (Fig. 2c). Therefore, both the extension of the Valencia Trough and a higher viscosity prefactor of the lower mantle are important for guiding the upright placement of the Gibraltar slab.

In conclusion, the simultaneous extension of the Valencia Trough and the Algerian Sea Basin represents a unique case of rifting linked with rotational subduction within a Mediterranean-style tectonic environment characterized by slowly converging plates and oblique subduction of a narrow oceanic basin coupled with irregular continental margins on both sides. This subduction system features an upright Gibraltar slab orientation

and rotational retreat of the trench, and the development of a pair of rift basins since the Oligocene, i.e., the Algerian Sea Basin and Valencia Trough, depends on the rheological nature of the continental margins and subducted lithosphere.

Methods

Numerical model setup

We formulated a series of time-evolving thermodynamic models with different initial constraints, viscosity layering prefactors, and crust yield coefficients via the finite element software Underworld2[47–49], which was used to solve the mass, momentum, and energy conservation equations for incompressible visco-plastic flow within a 3D Cartesian box (Fig. 2f–j). Our models incorporate the Boussinesq approximation, and we assume that density is influenced primarily by temperature perturbations, notwithstanding the intricate density differences among compositions. This relationship can be expressed as follows:

$$\rho_T = \rho_0 \left(1 - \alpha \left(T - T_0\right)\right), \tag{1}$$

where ρ is the density, α is the thermal expansion, and T is the temperature. The subscript 0 indicates the reference value. All the common physical parameters used in the models are shown in Supplementary Table 5.

The rheology of the materials in the models is determined by a combination of dislocation creep, diffusion creep, and plastic yielding[50–53] (Supplementary Table 1). In addition, the viscosity differences among different mantle layers are considered in the models[54]. The relationship between the average ductile viscosity and effective viscosity for diffusion and dislocation creep can be expressed as follows:

$$\eta_{ductile} = \begin{cases} \eta_{pre} * \left(\frac{1}{\eta_{diff}} + \frac{1}{\eta_{disl}}\right)^{-1} & depth \le 660 \, km \\ \eta_{pre} * \eta_{diff} & depth > 660 \, km \end{cases} \tag{2}$$

where η_{pre} is the viscosity prefactor for different layer depths[54] (Supplementary Table 2) and η_{diff} and η_{disl} are the viscosities for diffusion and dislocation creep[50], respectively.

η_{diff} can be calculated as follows:

$$\eta_{diff} = \frac{1}{2} A_D^{-1} \sigma_{crit}^{1-n} \exp\left(\frac{PV_a + E}{RT}\right), \tag{3}$$

where A_D is a prefactor, n is the power law exponent, P is the pressure, V_a is the activation volume, E is the activation energy, and R is the universal gas constant. σ_{crit} is the transition stress from diffusion to dislocation creep, and the value is 10 kPa[50,55].

The dislocation creep viscosity η_{disl} is assumed to obey a power law and it has similar parameters as the diffusion creep viscosity[56]:

$$\eta_{disl} = \frac{1}{2} A_D^{1/n} \dot{\varepsilon}_{II}^{(1-n)/n} \exp\left(\frac{PV_a + E}{nRT}\right), \tag{4}$$

where $\dot{\varepsilon}_{II}$ is the second invariant of the strain rate. The other values are the same as those for η_{diff}.

The Drucker–Prager yield criterion[51] was adopted to implement plasticity for rocks at shallow depths, so the final viscosity can be expressed as follows:

$$\eta = \left(\frac{1}{\eta_{yield}} + \frac{1}{\eta_{ductile}}\right)^{-1} \tag{5}$$

The yield viscosity η_{yield} can be calculated as follows:

$$\eta_{yield} = \frac{1}{2}\left(\frac{6 \sin \phi \, p}{\sqrt{3}(3 - \sin \phi)} + \frac{6C \cos \phi}{\sqrt{3}(3 - \sin \phi)}\right) \dot{\varepsilon}_{II}^{-1}, \tag{6}$$

where C is the cohesion, p is the lithostatic pressure, ϕ represents the friction angle, and $\dot{\varepsilon}_{II}$ is the second invariant of the strain rate. μ is the friction coefficient, which has the following relationship with ϕ:

$$\mu = \tan \phi. \tag{7}$$

We simply assume that the friction coefficient linearly decreases as the strain accumulates[52]:

$$\mu = \begin{cases} \mu_0 - \gamma\mu_\gamma, \gamma \le \gamma_0 \\ \mu_1, \gamma > \gamma_0 \end{cases}, \tag{8}$$

where μ_0 and μ_1 are the initial and final values, respectively; γ_0 is the upper strain limit for fracture-related weakening; and $\mu_\gamma = (\mu_0 - \mu_1)/\gamma_0$ is the rate at which the friction coefficient decreases. γ denotes the accumulated plastic strain and can be calculated as follows:

$$\gamma = \int \sqrt{\frac{1}{2}\dot{\varepsilon}_{ij(plastic)}^2} \, dt, \tag{9}$$

where t represents time and where $\dot{\varepsilon}_{ij(plastic)}$ represents the plastic strain rate tensor.

The 410 km and 660 km phase boundaries are incorporated into our models. The 660 km phase transition played a crucial role in preventing the slabs in the models from penetrating into the lower mantle and promoting slab stagnation. The setup for phase transitions in the model closely followed the approach used by Ref.[54].

The geodynamic model features resolutions of 130, 85, and 64 grid points in the longitude, latitude, and depth directions, respectively. To improve local resolution, we employed a mesh refinement method, achieving a horizontal resolution of 10 km near the southern margin of Iberia and around the Balearic Promontory, and a vertical resolution of 3–5 km above a depth of 80 km.

The model used free-slip boundary conditions and visco-plastic rheology was used. To help convergence and because the dynamic pressure is usually substantially smaller than the lithostatic pressure and the buffering effect of the small non-zero cohesion, dynamic pressure, instead of total pressure was used in calculating the yielding strength.

We used the MUMPS method[57] to solve the inner solver of the Stokes equations, which takes the majority of the solution time. The penalty value was set to 1×10^6, and the ksp_rtol value was set to 1×10^{-8}. The tolerance for the non-linear solver is 0.01.

All computations were performed via the AMD EPYC 64-core CPU at the Beijing Super Cloud Computing Center, with each model run taking approximately 14 days to complete on average.

We simulated the composition of the system using millions of Lagrangian particles uniformly dispersed throughout the box. Initially, each particle was assigned a composition on the basis of its depth and position, along with specific physical properties, such as density, activation energy, cohesion, and strain. As the model ran, the particles were transported by the local velocity field while retaining properties, such as density, rheological parameters (Supplementary Table 1) and accumulated strain. This parameter system has been widely used in previous geodynamic studies[50–53,56] and is consistent with the rheological assessment of the Gibraltar slab and surrounding mantle[34], which includes a strongly subducting slab and lithosphere (between $1 \times 10^{23} \, Pa \cdot s$ and $1 \times 10^{24} \, Pa \cdot s$), a weak mantle (between $1 \times 10^{20} \, Pa \cdot s$ and $1 \times 10^{22} \, Pa \cdot s$), and a lithospheric strength value in a weakened zone (e.g., North African margin, Valencia Trough and AlKaPeCa Domain) of approximately $1 \times 10^{21} \, Pa \cdot s$; this value is more than one order of magnitude

lower than that of the normal lithosphere. This set of rheological parameters can inhibit excessive stretching of the subducting slab and facilitate rifting at continental margins, providing conditions for the predicted slab geometry to match present-day seismic tomography models[34].

Constraints of the models with tectonics

To achieve improved spatial and temporal consistency with geological data, the initial conditions of our geodynamic models were constrained by plate reconstructions[58].

We assumed uniform crustal and lithospheric thicknesses and compositions for the continents, with their temperature fields increasing linearly with depth, reaching 680 K at the bottom of the crust and 1330 K at the base of the lithosphere[50] (Fig. 2j). Additionally, a half-space cooling model[55] was adopted for the temperature fields in the oceanic basins, where the temperature depended on the age of the oceanic lithosphere and depth to the surface. For the subducted slabs, we assumed a quarter-circular shape with a 200 km radius from the trench at the surface that dips into the upper mantle in any profile perpendicular to the trench strike (Fig. 2g). It was also assumed that the slabs consisted purely of oceanic crust and lithosphere, and their temperature fields also followed that of the half-space cooling model. We set a low-viscosity oceanic crustal layer as the entrained weak layer[54,59,60] that facilitated continuous decoupling between the subducting slab and the overlying plate near the trench. A free-slip velocity boundary condition was applied to the surface, and the entire system was driven primarily by the negative buoyancy of the slabs throughout the model run.

The models spanned from 7°W to 8°E in the east-west direction, from 31°N to 42°N in the north-south direction (Fig. 1), and from the surface to a depth of 1000 km in the vertical direction. This volume covered most of the Iberian Peninsula, the African margin to the north of the Atlas (Fig. 1), and the Mediterranean coast between the two continents; this coverage enabled modeling of the Gibraltar subduction zone. With the aid of mesh refinement, the maximum resolution values in key areas, such as the Liguro-Tethys Ocean (Fig. 2) and the Iberian margin along the Betics-Balearic Promontory (Fig. 1), were set to less than 5 km, facilitating modeling of the dynamic subduction process of the Gibraltar slab with a relatively low computational burden.

We constrained the configuration of the continent and ocean based on a global tectonic reconstruction model[61] at 30 Ma, assuming a fixed Iberian continent. According to this model, the ocean basin between Africa and Iberia was approximately 150 km wider on average than it is today. Although some researchers have argued that fully mature oceanic crust may not have been present at the margin between Africa and Iberia[62], we treated the lithosphere that had already been consumed between the continents as oceanic lithosphere. This approximation was reasonable since only a sufficiently negatively buoyant oceanic crust could provide the driving force for ongoing subduction[63]. Furthermore, we approximated the age of the subducted oceanic crust as 100 Myr, corresponding to the age of the Cretaceous drifting event between Africa and Europe[64]. These approximations ensured consistency between the negative buoyancy of the subducted slabs in the model and that of the real geodynamic history.

Since the subduction history of the Gibraltar subduction zone is still a matter of debate (Supplementary text), we compiled and digitized four previously published representative reconstruction models in GIS software to delineate the original geography of continents and oceans, as well as the distributions of various features, such as trenches, weak zones, and fracture zones, in the mid-Oligocene (Fig. 2b-e). Additionally, we created a fifth reconstruction model, referred to as the reconstruction model M23 (Fig. 2a).

The reconstruction of M23 is based on existing observations of surface and deep mantle structures, combined with a previously proposed reconstruction model by Spakman and Wortel[33]. The initial setup of the model considered the tectonic evolution of the Betic orogeny, the Valencia Trough, the African margin, and the deep slab structure, with a particular focus on explaining the deformation sequence of the Balearic Islands. The initial polarity of the Gibraltar subducting slab was oriented northeastward. We restored the Valencia Trough to its pre-extension state and introduced weak zones along the axis of the basin, which currently features the deepest bathymetry and thinned crust. During the model run, these predefined weak zones underwent preferential extensional deformation under the influence of subduction activity, thereby modifying the stress field and influencing the final evolution of the subduction zone. This design aligns with the fundamental tectonic framework of the region, with the aim of specifically addressing the rationality of an ENE-dipping subduction and the impact of the development of the Valencia Trough on the geodynamic evolution of the region.

The digitized datasets of these five reconstruction models served as initial constraints for establishing the initial material and temperature field conditions in the geodynamic models (Fig. 2f-j).

Quantitative validation of model predictions

To evaluate the feasibility of the geodynamic model cases, we conducted a quantitative analysis to evaluate the consistency between the predicted Gibraltar slab and the high-velocity anomalies interpreted from seismic tomographic model UU-P07[31] along four profiles, which cross the major tectonic belts orthogonally in different directions (Fig. 1). We assumed that the velocity anomalies were related primarily to the temperature perturbations. To avoid the influence of surface boundaries, our analysis focused only on the mantle below 100 km depth. For each case in each profile, we initially divided the model domain into two subdivisions: subdivision A, representing the cold slab (15% below the background temperature), and subdivision B, representing the ambient mantle temperature. Additionally, on the basis of tomographic slice data (Supplementary Fig. 24a), we further divided the domain into subdivision C (the suspected slab area with velocity anomalies higher than 0.3%) and subdivision D (the nonslab area with velocity anomalies lower than 0.3%). The four subdivision pairs (AC, BC, AD, and BD) were utilized to assess the success of the model predictions (Supplementary Fig. 24b–d). For example, subdivision AC may indicate the overlapping region between the low-temperature region predicted by the geodynamic model and the suspected slab area shown by UU-P07. The two scores, R_1 and R_2, were subsequently calculated as follows:

$$R_1 = \frac{A_{AC}}{A_{AC} + A_{AD}} \times 100\%, \tag{10}$$

$$R_2 = \frac{A_{AC}}{A_{AC} + A_{BC}} \times 100\%, \tag{11}$$

where A_{AC}, A_{AD} and A_{BC} correspond to the areas of subdivisions AC, AD and BC, respectively.

A higher R_1 value signifies that a greater proportion of the predicted slabs fall within the high-velocity anomalies in tomography model UU-P07, whereas a higher R_2 value indicates that a greater proportion of high-velocity anomalies are predicted by geodynamic models. Cases demonstrating higher R_1 and R_2 scores may indicate better alignment with the tomographic model for a particular profile. Finally, the prediction accuracies for all the profiles in all the cases were statistically analyzed (Supplementary Fig. 3 and Supplementary Table 4).

Data availability

The output data files of the models have been deposited in the figshare repository. The DOI number of the dataset is https://doi.org/10.6084/m9.figshare.25359238. The data can be accessed by the following url link: https://figshare.com/s/fcb97f91bd6b51349ce9.

Code availability

Numerical simulation code is available at https://underworld2.readthedocs.io/en/latest/, the version we used is 2.12.5. The custom code for the model can be accessed by contacting the corresponding authors. The code used to make the figures can be accessed at https://www.generic-mapping-tools.org/ and https://www.paraview.org/.

Article

References

1. Conrad, C. P. & Lithgow-Bertelloni, C. How mantle slabs drive plate tectonics. *Science* **298**, 207–209 (2002).
2. Becker, T. W. & O'Connell, R. J. Predicting plate velocities with mantle circulation models. *Geochem. Geophys. Geosyst.* **2**, 1060 (2001).
3. Coltice, N., Husson, L., Faccenna, C. & Arnould, M. What drives tectonic plates? *Sci Adv* **5**, eaax4295 (2019).
4. Husson, L. Trench migration and upper plate strain over a convecting mantle. *Phys. Earth Planet. Inter.* **212-213**, 32–43 (2012).
5. Schellart, W. P., Chen, Z., Strak, V., Duarte, J. C. & Rosas, F. M. Pacific subduction control on Asian continental deformation including Tibetan extension and Eastward extrusion tectonics. *Nat. Commun.* **10**, 4480 (2019).
6. Menant, A., Sternai, P., Jolivet, L., Guillou-Frottier, L. & Gerya, T. 3D numerical modeling of mantle flow, crustal dynamics and magma genesis associated with slab roll-back and tearing: the Eastern Mediterranean case. *Earth Planet. Sci. Lett.* **442**, 93–107 (2016).
7. Karig, D. E. Origin and development of marginal basins in the Western Pacific. *J. Geophys. Res.* **76**, 2542–2561 (1971).
8. Balázs, A., Faccenna, C., Gerya, T., Ueda, K. & Funiciello, F. The dynamics of forearc—back-arc basin subsidence: numerical models and observations from Mediterranean subduction zones. *Tectonics* **41**, e2021TC007078 (2022).
9. Jolivet, L., Faccenna, C., D'Agostino, N., Fournier, M. & Worrall, D. The kinematics of back-arc basins, examples from the Tyrrhenian, Aegean and Japan Seas. *Geol. Soc. Lond. Spec. Publ.* **164**, 21–53 (2022).
10. Schliffke, N., van Hunen, J., Allen, M. B., Magni, V. & Gueydan, F. Episodic back-arc spreading centre jumps controlled by transform fault to overriding plate strength ratio. *Nat. Commun.* **13**, 582 (2022).
11. Magni, V., Faccenna, C., van Hunen, J. & Funiciello, F. How collision triggers backarc extension: insight into Mediterranean style of extension from 3-D numerical models. *Geology* **42**, 511–514 (2014).
12. Sdrolias, M., Müller, R. D., Mauffret, A. & Bernardel, G. Enigmatic formation of the Norfolk basin, SW Pacific: a plume influence on back-arc extension. *Geochem. Geophys. Geosyst.* **5**, Q06005 (2004).
13. Faccenna, C., Funiciello, F., Giardini, D. & Lucente, P. Episodic back-arc extension during restricted mantle convection in the Central Mediterranean. *Earth Planet. Sci. Lett.* **187**, 105–116 (2001).
14. Hall, R. Cenozoic geological and plate tectonic evolution of SE Asia and the SW Pacific: computer-based reconstructions, model and animations. *J. Asian Earth Sci.* **20**, 353–431 (2002).
15. Faccenna, C., Becker, T. W., Lucente, F. P., Jolivet, L. & Rossetti, F. History of subduction and back-arc extension in the central Mediterranean. *Geophys. J. Int.* **145**, 809–820 (2001).
16. Jolivet, L. et al. Geodynamic evolution of a wide plate boundary in the Western Mediterranean, near-field versus far-field interactions. *Bull. Soc. Géol. Fr.* **192**, 48 (2021).
17. Romagny, A. et al. Detailed tectonic reconstructions of the Western Mediterranean region for the last 35 Ma, insights on driving mechanisms. *Bull. Soc. Géologique France* **191**, 37 (2020).
18. de la Peña, L. G., Ranero, C. R., Gràcia, E. & Booth-Rea, G. The evolution of the Westernmost Mediterranean basins. *Earth Sci. Rev.* **214**, 103445 (2021).
19. Ayala, C., Torne, M. & Roca, E. A review of the current knowledge of the crustal and lithospheric structure of the Valencia Trough basin. *Bol. Geol. Min.* **126**, 533–552 (2015).
20. van Hinsbergen, D. J. J., Vissers, R. L. M. & Spakman, W. Origin and consequences of western Mediterranean subduction, rollback, and slab segmentation. *Tectonics* **33**, 393–419 (2014).
21. Vergés, J. & Fernàndez, M. Tethys–Atlantic interaction along the Iberia–Africa plate boundary: The Betic–Rif orogenic system. *Tectonophysics* **579**, 144–172 (2012).
22. Banda, E. & Santanach, P. The Valencia trough (western Mediterranean): An overview. *Tectonophysics* **208**, 183–202 (1992).
23. Vergés, J. C. & Sàbat, F. Constraints on the Neogene Mediterranean kinematic evolution along a 1000 km transect from Iberia to Africa. *Geol. Soc. Lond. Spec. Publ* **156**, 63–80 (1999).
24. Jolivet, L. et al. Fast dismantling of a mountain belt by mantle flow: Late-orogenic evolution of Pyrenees and Liguro-Provençal rifting. *Tectonophysics* **776**, 228312 (2020).
25. Moragues, L. et al. Two Cenozoic extensional phases in Mallorca and their bearing on the geodynamic evolution of the Western Mediterranean. *Tectonics* **40**, e2021TC006868 (2021).
26. Do Couto, D. et al. Tectonic and stratigraphic evolution of the Western Alboran Sea Basin in the last 25 Myrs. *Tectonophysics* **677-678**, 280–311 (2016).
27. Mauffret, A., de Lamotte, D. F., Lallemant, S., Gorini, C. & Maillard, A. E. –W. opening of the Algerian basin (Western Mediterranean). *Terra Nova* **16**, 257–264 (2004).
28. Haidar, S. et al. Back-Arc Dynamics Controlled by Slab Rollback and Tearing: A Reappraisal of Seafloor Spreading and Kinematic Evolution of the Eastern Algero-Balearic Basin (Western Mediterranean) in the Middle-Late Miocene. *Tectonics* **41**, e2021TC006877 (2022).
29. Booth-Rea, G., Ranero, C. R., Martínez-Martínez, J. M. & Grevemeyer, I. Crustal types and Tertiary tectonic evolution of the Alborán Sea, western Mediterranean. *Geochem. Geophys. Geosyst.* **8**, Q10005 (2007).
30. Bezada, M. J. et al. Evidence for slab rollback in Westernmost Mediterranean from improved upper mantle imaging. *Earth Planet. Sci. Lett.* **368**, 51–60 (2013).
31. Hall, R. & Spakman, W. Mantle structure and tectonic history of SE Asia. *Tectonophysics* **658**, 14–45 (2015).
32. Rosenbaum, G., Lister, G. & Duboz, C. Reconstruction of the tectonic evolution of the Western Mediterranean since the Oligocene. *J. Virtual Explor.* **8**, 107–130 (2002).
33. Spakman, W. & Wortel, R. in *The TRANSMED Atlas. The Mediterranean Region from Crust to Mantle: Geological and Geophysical Framework of the Mediterranean and the Surrounding Areas* (eds. Cavazza, W., Roure, F., Spakman, W., Stampfli, G. M. & Ziegler, P. A.) 31–52 (Springer Berlin Heidelberg, 2004).
34. Chertova, M. V., Spakman, W., Geenen, T., van den Berg, A. P. & van Hinsbergen, D. J. J. Underpinning tectonic reconstructions of the western Mediterranean region with dynamic slab evolution from 3-D numerical modeling. *J. Geophys. Res.: Solid Earth* **119**, 5876–5902 (2014).
35. Peral, M., Fernàndez, M., Vergés, J., Zlotnik, S. & Jiménez-Munt, I. Numerical modelling of opposing subduction in the Western Mediterranean. *Tectonophysics* **830**, 229309 (2022).
36. Duarte, J. C. et al. Gibraltar subduction zone is invading the Atlantic. *Geology* **52**, 331–335 (2024).
37. Civiero, C. et al. A common deep source for upper-mantle upwellings below the Ibero-western Maghreb region from teleseismic P-wave travel-time tomography. *Earth Planet. Sci. Lett.* **499**, 157–172 (2018).
38. d'Acremont, E. et al. Polyphase tectonic evolution of fore-arc basin related to STEP fault as revealed by seismic reflection data from the Alboran Sea (W-Mediterranean). *Tectonics* **39**, e2019TC005885 (2020).
39. Fontboté, J. M. et al. The Cenozoic geodynamic evolution of the Valencia Trough (Western Mediterranean). *Rev. Soc. Geol. Esp.* **3**, 7–18 (1990).
40. Schellart, W. P. & Moresi, L. A new driving mechanism for backarc extension and backarc shortening through slab sinking induced toroidal and poloidal mantle flow: results from dynamic subduction models with an overriding plate. *J. Geophys. Res. Solid Earth* **118**, 3221–3248 (2013).
41. van den Broek, J. M., Magni, V., Gaina, C. & Buiter, S. J. H. The formation of continental fragments in subduction settings: the importance of structural inheritance and subduction system dynamics. *J. Geophys. Res. Solid Earth* **125**, e2019JB018370 (2020).

42. Etheve, N. et al. Extreme Mesozoic crustal thinning in the Eastern Iberia margin: the example of the Columbrets Basin (Valencia Trough). *Tectonics* **37**, 636–662 (2018).

43. Villaseñor, A. et al. Subduction and volcanism in the Iberia–North Africa collision zone from tomographic images of the upper mantle. *Tectonophysics* **663**, 238–249 (2015).

44. Obayashi, M. et al. Finite frequency whole mantle P wave tomography: improvement of subducted slab images. *Geophys. Res. Lett.* **40**, 5652–5657 (2013).

45. Li, C., van der Hilst, R. D., Engdahl, E. R. & Burdick, S. A new global model for P wave speed variations in Earth's mantle. *Geochem. Geophys. Geosystems* **9**, Q05018 (2008).

46. Goes, S., Agrusta, R., van Hunen, J. & Garel, F. Subduction-transition zone interaction: a review. *Geosphere* **13**, 644–664 (2017).

47. Moresi, L. et al. Computational approaches to studying non-linear dynamics of the crust and mantle. *Phys. Earth Planet. Inter.* **163**, 69–82 (2007).

48. Moresi, L., Betts, P. G., Miller, M. S. & Cayley, R. A. Dynamics of continental accretion. *Nature* **508**, 245–248 (2014).

49. Mansour, J. G. et al. Underworld2: Python Geodynamics Modelling for Desktop, HPC and Cloud. *Journal of Open Source Software* **5**, 1–3 (2020).

50. Balázs, A. et al. Oblique subduction and mantle flow control on upper plate deformation: 3D geodynamic modeling. *Earth Planet. Sci. Lett.* **569**, 117056 (2021).

51. Ranalli, G. *Rheology of the Earth* (Springer Science & Business Media, 1995).

52. Munch, J., Gerya, T. & Ueda, K. Oceanic crust recycling controlled by weakening at slab edges. *Nat. Commun.* **11**, 2009 (2020).

53. Gerya, T. V., Stern, R. J., Baes, M., Sobolev, S. V. & Whattam, S. A. Plate tectonics on the Earth triggered by plume-induced subduction initiation. *Nature* **527**, 221–225 (2015).

54. Yang, T., Liu, S., Guo, P., Leng, W. & Yang, A. Yanshanian Orogeny During North China's Drifting Away From the Trench: Implications of Numerical Models. *Tectonics* **39**, e2020TC006350 (2020).

55. Turcotte, D. L. & Schubert, G. *Geodynamics* (Cambridge University Press, 2002).

56. Gerya, T. V. & Yuen, D. A. Robust characteristics method for modelling multiphase visco-elasto-plastic thermo-mechanical problems. *Phys. Earth Planet. Int.* **163**, 83–105 (2007).

57. Amestoy, P. R., Guermouche, A., L'Excellent, J.-Y. & Pralet, S. Hybrid scheduling for the parallel solution of linear systems. *Parallel Comput.* **32**, 136–156 (2006).

58. Bower, D. J., Gurnis, M. & Flament, N. Assimilating lithosphere and slab history in 4-D Earth models. *Phys. Earth Planet. Inter.* **238**, 8–22 (2015).

59. Sandiford, D. & Moresi, L. Improving subduction interface implementation in dynamic numerical models. *Solid Earth* **10**, 969–985 (2019).

60. Yang, T., Moresi, L., Zhao, D., Sandiford, D. & Whittaker, J. Cenozoic lithospheric deformation in Northeast Asia and the rapidly-aging Pacific plate. *Earth Planet. Sci. Lett.* **492**, 1–11 (2018).

61. Müller, R. D. et al. A global plate model including lithospheric deformation along major rifts and orogens since the Triassic. *Tectonics* **38**, 1884–1907 (2019).

62. Pedrera, A. et al. Evolution of the South-Iberian paleomargin: from hyperextension to continental subduction. *J. Struct. Geol.* **138**, 104122 (2020).

63. Faccenna, C., Piromallo, C., Crespo-Blanc, A., Jolivet, L. & Rossetti, F. Lateral slab deformation and the origin of the Western Mediterranean arcs. *Tectonics* **23**, TC1012 (2004).

64. Schettino, A. & Turco, E. Tectonic history of the Western Tethys since the late Triassic. *Geol. Soc. Am. Bull.* **123**, 89–105 (2010).

65. Amante, C. & Eakins, B. W. ETOPO1 1 Arc Minute Global Relief Model: Procedures, Data Sources and Analysis. *NOAA Technical Memorandum NESDIS NGDC-24* (2009).

Author contributions
P.M.: conceptualization, methodology, software, result analysis, investigation, writing of the original draft, and visualization. S.L.: supervision, formal analysis and discussion, writing of the original draft, review and editing. G.B.: review and editing. H.Z.: review and editing. T.Y.: methodology, software, visualization, result analysis, review and editing.

Competing interests
The authors declare no competing interests.

Additional information
Supplementary information The online version contains supplementary material available at https://doi.org/10.1038/s43247-024-01833-6.

Correspondence and requests for materials should be addressed to Pengfei Ma or Shaofeng Liu.

Peer review information *Communications Earth and Environment* thanks Boris Kaus, Agnès Maillard reviewers for their contribution to the peer review of this work. Primary Handling Editors: Joao Duarte and Carolina Ortiz Guerrero. A peer review file is available.

Reprints and permissions information is available at http://www.nature.com/reprints

Publisher's note Springer Nature remains neutral with regard to jurisdictional claims in published maps and institutional affiliations.